

SCIENTIFIC REPORTS



OPEN

Microwave index engineering for slow-wave coplanar waveguides

Álvaro Rosa¹, Steven Verstuyft², Antoine Brimont¹, Dries Van Thourhout² & Pablo Sanchis¹

Received: 19 January 2018

Accepted: 19 March 2018

Published online: 04 April 2018

Microwave index engineering has been investigated in order to properly design slow-wave coplanar waveguides suitable for a wide range of applications in microwave, photonics, plasmonics and metamaterials. The introduction and optimization of novel capacitive and inductive elements is proposed as a design approach to increase the microwave index while keeping the impedance close to 50 Ω to ensure the compatibility with external electronic devices. The contribution of inductive and capacitive elements and their influence on the performance of the slow-wave coplanar waveguide has been systematically analyzed. As a result, a microwave index as high as 11.6 has been experimentally demonstrated in a frequency range up to 40 GHz which is, to the best of our knowledge, the largest microwave index obtained so far in coplanar waveguides.

Monolithic coplanar waveguides (CPWs) play a key role in integrated devices technology. CPWs can be used for many applications due to their planar geometry (both ground and signal are in the same plane) that reduces the fabrication complexity and makes them compatible with a large variety of structures and applications. Furthermore, CPWs exhibit a very low dispersion, and thus broadband performance, owing to its fundamental quasi-TEM propagation mode^{1,2}. Slow-wave CPWs can be viewed as an alternative to regular CPW which allows the slowdown of the propagation velocity as well as the electrical length reduction^{3–5}. Therefore, slow-wave CPWs are of paramount importance in several fields such as microwaves, photonics, plasmonics and metamaterials. In the microwave field, slow-wave CPWs are used to design new compact delay lines⁶, phase shifters or microwave filters^{7–11} with an important size reduction in comparison with regular CPWs. In plasmonics, slow-wave CPWs have been used for designing and modelling new spoof surface plasmon modes^{12–14}. Moreover the management of the microwave index as well as the impedance is an essential target in metamaterials^{15,16} with several applications like compact multilayer transmission lines, negative and zero order resonator or lens design among others^{16,17}. Finally, regarding to the photonic field, slow-wave electro-optic modulators have been reported to reduce the drive voltage and footprint^{18–25}. However, slow wave CPWs are required for matching microwave and optical indices to avoid a reduction of the electro-optic modulation bandwidth²².

Appropriate tuning of the microwave index of the slow-wave CPW can therefore be beneficial in many fields and applications. The majority of works focus on increasing the capacitance of the CPW as the main method to enlarge the microwave index^{9–11,20,23–27}. Here, we propose an improved approach to properly design a high microwave index in slow-wave CPWs by increasing both capacitance and inductance. In such a way, we are able to demonstrate a gradual increase of the microwave index, reaching the highest value reported so far to the best of our knowledge. Furthermore, the influence of the capacitive and inductive elements on the impedance, to ensure a slow-wave CPW compatible with the standard 50 Ω characteristic impedance, is also considered. The proposed slow-wave CPW features broadband performance with a bandwidth extending beyond 40 GHz.

Microwave theory and proposed design approach

To address the design of slow-wave CPWs, it is necessary to lay down the basis of microwave theory. This includes basically the transmission line theory to understand the transmission behaviour, and the conformal mapping technique to analyze the influence of the different parameters in a CPW. Figure 1(a) shows the equivalent circuit of a CPW while Fig. 1(b) depicts the transversal view of the CPW with the key design parameters.

The CPW has an inductive and capacitive behaviour, as can be seen in Fig. 1(a), so that from the transmission line theory we can obtain the relationship between the microwave index and the impedance with the capacitance, C , and the inductance, L . That relationship is expressed by the following equations²:

¹Nanophotonics Technology Center, Universitat Politècnica de València, Camino de Vera s/n, Valencia, 46022, Spain. ²Photonics Research Group, Department of Information Technology (INTEC), Ghent University–imec, Technologiepark-Zwijnaarde 15, Gent, B-9052, Belgium. Correspondence and requests for materials should be addressed to Á.R. (email: alroes3@ntc.upv.es) or P.S. (email: pabsanki@ntc.upv.es)

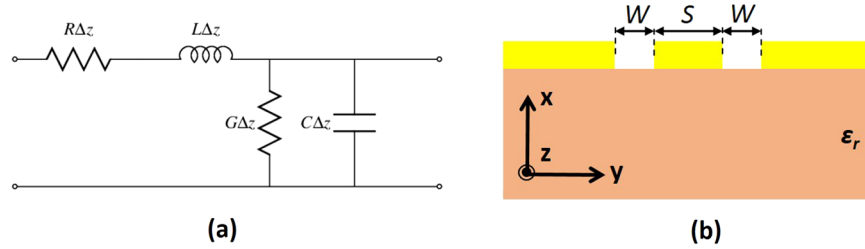


Figure 1. (a) Equivalent circuit model and (b) transversal view of a CPW.

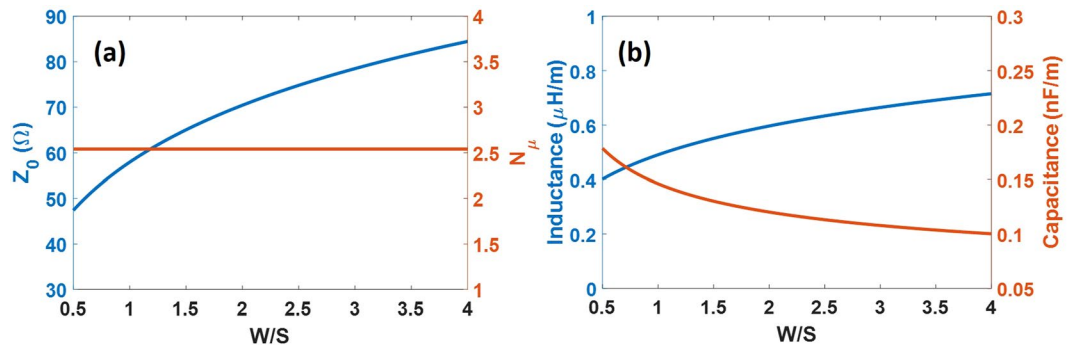


Figure 2. (a) Impedance and the microwave index, and (b) capacitance and the inductance as a function of W/S obtained by the conformal mapping method.

$$Z_0 = \sqrt{\frac{L}{C}} \tag{1}$$

$$N_\mu = c_0 \sqrt{LC} \tag{2}$$

where Z_0 is the impedance, N_μ is the microwave index, c_0 is the speed of light in vacuum, L is the inductance and C is the capacitance. On the other hand, the conformal mapping method links these characteristic parameters of the transmission line with the physical parameters of the CPW^{28,29} like the central strip width or the gap between signal and ground planes, shown in Fig. 1(b):

$$C_{CPW} = 2\varepsilon_0(\varepsilon_r + 1) \frac{K(k_0)}{K(\sqrt{1 - k_0^2})} \tag{3}$$

$$L_{CPW} = \frac{1}{4c_0^2\varepsilon_0} \frac{K(\sqrt{1 - k_0^2})}{K(k_0)} \tag{4}$$

where $K(k)$ represents a complete elliptic integral of the first kind²⁹, ε_r is the relative permittivity of the substrate, ε_0 is the vacuum permittivity and

$$k_0 = \frac{1}{1 + 2(W/S)} \tag{5}$$

where W is the gap and S the central strip width of the coplanar waveguide. Therefore, taking into account equations (1)–(5) is possible to obtain the impedance and the microwave index for a regular CPW of given dimensions. Figure 2 shows the influence of W/S on the impedance and microwave index as well as on the inductance and capacitance for a silicon substrate ($\varepsilon_r = 11.9$).

As can be seen in Fig. 2(a), the impedance increases when W/S increases. However, the microwave index remains constant over the whole W/S range because the reduction of the capacitance is balanced by the larger inductance (Fig. 2(b)). In previous works^{10,11,20,23–26}, the introduction of periodic capacitive elements (thin fins) to the CPW has been proposed to increase the capacitance without decreasing the inductance, which results in a microwave index increase and an impedance reduction. This is an effective method but does not take into account the inductance as a parameter that may also be exploited for the design. In order to manipulate the inductance, the CPW strips can be reduced by using periodic thin slots. The proposed slots allow the inductance to be increased while only having a small effect on the capacitance. Therefore, increasing the inductance can be

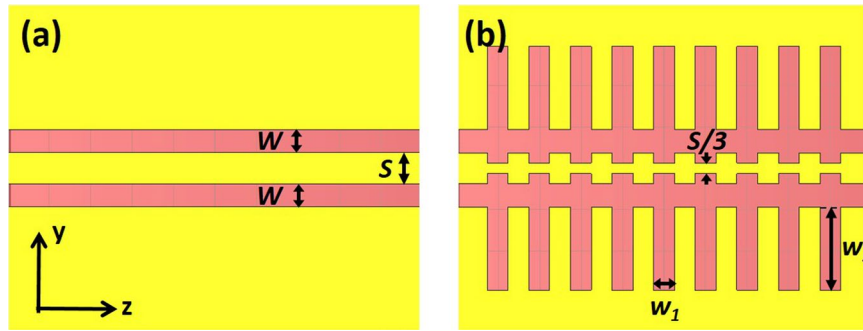


Figure 3. (a) Top view of a regular CPW and (b) of a slow-wave CPW.

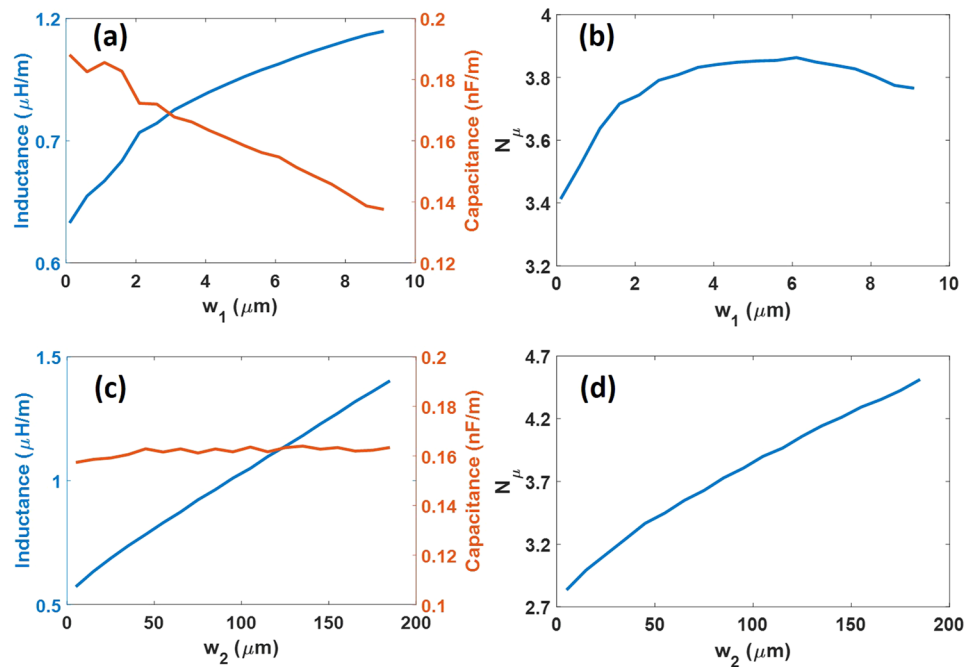


Figure 4. (a) Simulated inductance and capacitance and (b) microwave index as a function of w_1 and $w_2 = 100 \mu\text{m}$ and (c) simulated inductance and capacitance and (d) microwave index as a function of w_2 and $w_1 = 5 \mu\text{m}$ for the slow-wave CPW shown in Fig. 3(b).

combined with approaches based on increasing the capacitance. Such a combination will allow us to reaching much higher microwave indices, while keeping the impedance close to 50Ω .

To design the slow-wave CPW, it is crucial to analyze the thin slots in order to understand their influence on the inductance and the capacitance and therefore on the microwave index. The analysis has been carried out using the electromagnetic simulation software CST microwave studio. CST is a simulation tool that solves Maxwell equations for each point on a 2D or 3D mesh using a finite elements method. The frequency has been fixed at 20 GHz. Figure 3 shows a top view of the regular and slow-wave CPWs with the parameters to be designed. For the regular CPW, $S = 15 \mu\text{m}$ and $W = 11 \mu\text{m}$ so that $W/S = 0.73$. By properly checking Fig. 2(a), an impedance value close to 50Ω is achieved.

Figure 3(b) depicts the proposed slots to increase the inductance, where w_1 and w_2 are the length and width of the slot. The period of the slots has been previously optimized to $20 \mu\text{m}$. The variation of the capacitance and inductance as a function of w_1 is shown in Fig. 4(a) for $w_2 = 100 \mu\text{m}$. It can be seen that there is an opposite behavior between them. The increase of the inductance is higher than the capacitance reduction, resulting in a microwave index increment (Fig. 4(b)). However, the increase of the inductance is not constant with w_1 so that the increase of the microwave index is reduced for larger w_1 values. On the other hand, the behavior of the capacitance and the inductance with w_2 is shown in Fig. 4(c), for $w_1 = 5 \mu\text{m}$. While the inductance increases with w_2 , the capacitance remains constant, which gives rise to higher microwave index with larger w_2 , as it can be seen in Fig. 4(d).

Figure 5(a) shows the impedance as a function of w_1 and w_2 . The corresponding microwave index is depicted in Fig. 5(b). It can be seen that larger microwave indices are achieved at the expense of increasing the impedance,

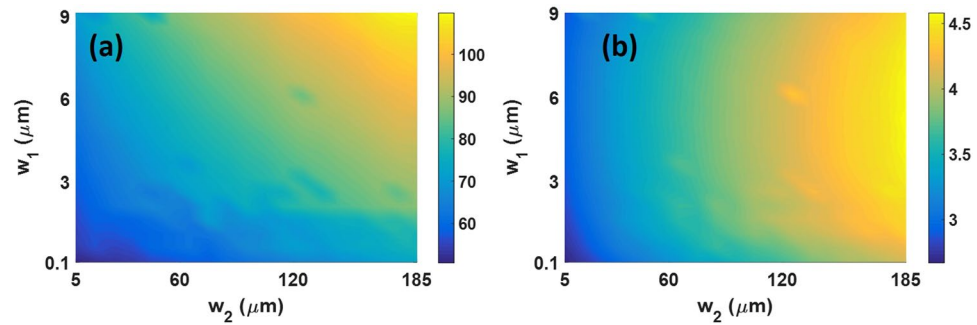


Figure 5. (a) Impedance and (b) microwave index as a function of w_1 and w_2 .

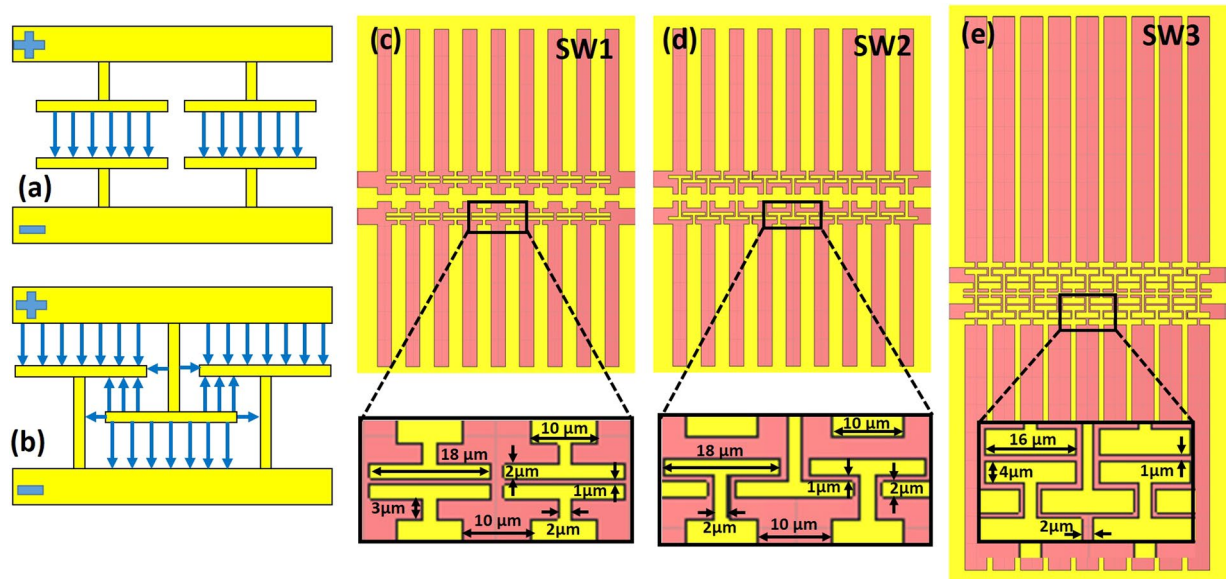


Figure 6. Schematic of (a) parallel and (b) novel crossed T-rails to increase the capacitance of the CPW. The blue lines represent the induced electric field due to the T-rails. Slow-wave CPW with (c) parallel T-rails, (d) crossed T-rails and (e) a combination of both configurations for improved performance.

which is in agreement with equation (1) as the inductance increase dominates over the capacitance. Therefore, it is clear that the proposed slots act as enhanced inductive elements in the slow-wave CPW. However, to keep the impedance close to 50Ω without reducing the microwave index, the introduction of capacitive elements is also required. The capacitance can be increased with the introduction of parallel T-rails, as shown in Fig. 6(a), which are periodically repeated along the propagation direction^{21–24}. A novel approach based on a crossed T-rail, as depicted in Fig. 6(b), is here also proposed to further increase the capacitance. The induced electric field due to the T-rails is represented with blue lines in Fig. 6(a,b).

Parallel T-rails with a length of $18 \mu\text{m}$, width of $2 \mu\text{m}$ and gap of $1 \mu\text{m}$ have been added on the inductive slow-wave CPW with $w_1 = 5 \mu\text{m}$ and $w_2 = 100 \mu\text{m}$. The slow-wave CPW is shown in Fig. 6(c) and has been named as SW1. The same inductive slow-wave CPW but with the crossed T-rails has also been considered to evaluate the difference in capacitance and so the influence on the microwave index. In this case, the CPW is depicted in Fig. 6(d) and has been named as SW2. Finally, a slow-wave CPW with a combination of both crossed and parallel T-rails, named as SW3 and shown in Fig. 6(e), has also been designed to further improve the capacitance. The length and width of the T-rails have been optimized to $16 \mu\text{m}$ and $4 \mu\text{m}$, respectively. Furthermore, the inductive performance has been enhanced by changing w_1 to $17 \mu\text{m}$ and w_2 to $180 \mu\text{m}$. As the capacitance of the slow-wave CPW is ruled by the capacitive T-rail elements, the reduction of the capacitance due to the larger w_1 is negligible.

Figure 7 shows the simulation results for the different designs of the slow-wave CPWs. SW0 refers to the inductive slow-wave CPW shown in Fig. 3(b) with $w_1 = 5 \mu\text{m}$ and $w_2 = 100 \mu\text{m}$. The capacitive and inductive behavior of the slow-wave CPWs are depicted in Fig. 7(a). The capacitance is gradually improved up to a factor of four (from 0.2 to 0.8 nF/m) by the introduction of the capacitive T-rail elements in SW1 and their modifications in SW2 and SW3. The inductance is approximately constant for SW0, SW1 and SW2, but it increases from 1.05 to $1.67 \mu\text{H/m}$ for SW3 due to the changes in the ground slots and the modification of the signal strip. The impedance, Fig. 7(b), and microwave index, Fig. 7(c), will be determined by the capacitive and inductive behavior.

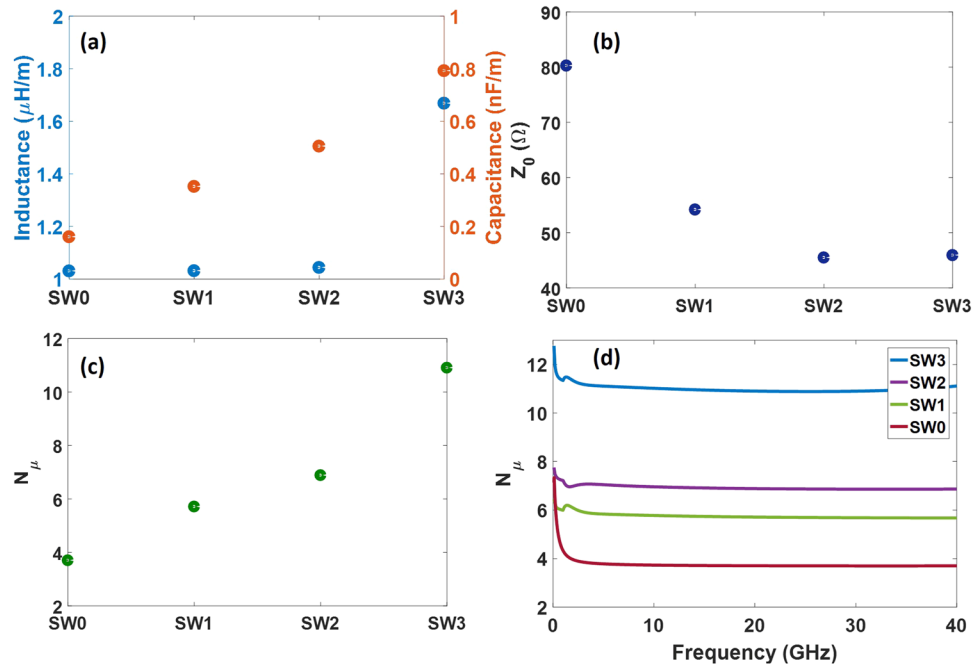


Figure 7. (a) Inductance and capacitance, (b) impedance and (c) microwave index for the different designs of the slow-wave CPWs obtained by simulations at 20 GHz. (d) Simulated microwave index as a function of the frequency.

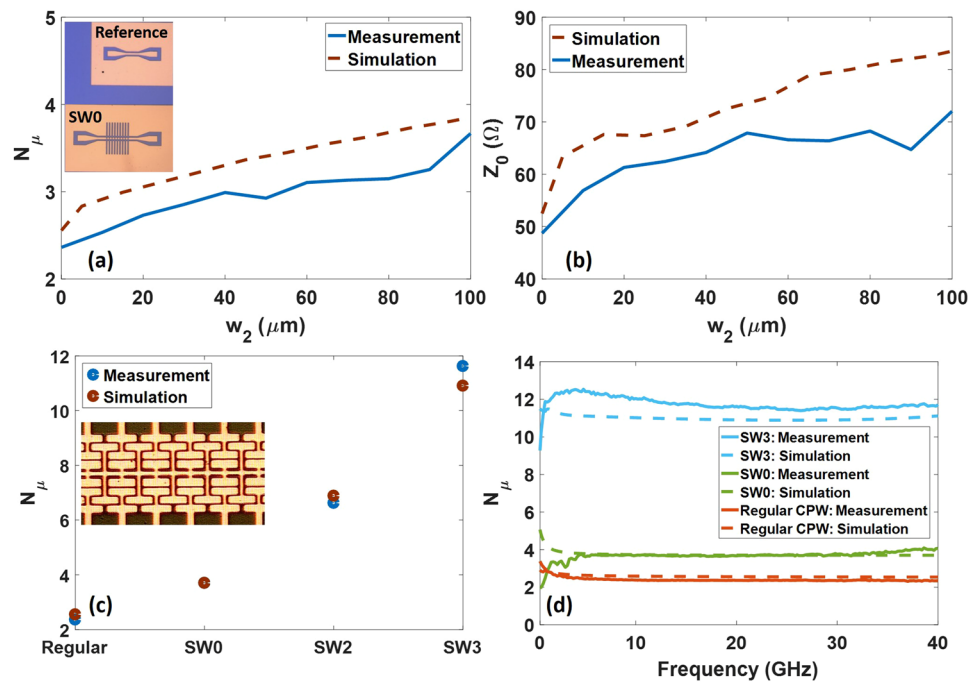


Figure 8. (a) Simulated and measured microwave index and (b) impedance for SW0 as a function of w_2 and assuming $w_1 = 5 \mu\text{m}$. An inset with an optical view of the reference CPW and SW0 with $w_2 = 100 \mu\text{m}$ is included. Simulated and measured microwave index (c) at 20 GHz for the regular CPW, SW0, SW2 and SW3 and (d) as a function of frequency for the regular CPW, SW0 and SW3. The inset in (c) shows an optical view of the fabricated SW3.

The impedance is decreased to a value close to 50Ω for the improved designs of the slow-wave CPWs due to the larger capacitance with respect to the original design of SW0. The microwave index is also increased for SW1 and SW2 due to the larger capacitance but the improvement is much larger for SW3 due to the additional increase of

Reference	Year	Structure	$N\mu$	α (dB/mm)	Z_0 (Ω)
⁵	2005	CPW	4.47	4–6.9	50
⁹	2013	CPW	5.3	0.7	35
¹¹	2001	CPW	3.74	—	50
¹⁹	1994	CPW	3.15	40	50
²⁰	2017	CPW	3.9	2	50
²¹	1996	CPW	2.6	46	50
²³	2011	CPW	4	33	50
²⁴	1993	CPW	3.4	—	50
²⁵	1995	CPW	3.37	2	45
²⁶	2009	CPW	5.9	0.4	43
²⁷	2015	CPW	7.38	1.4	34
This work (CPW)	2018	CPW	2.5	0.25	50
This work (SW0)	2018	CPW	3.7	0.6	80
This work (SW3)	2018	CPW	11.6	5.4	50

Table 1. Microwave index, propagation losses and impedance comparison for reported slow-wave transmission lines.

the inductance. Thereby, the microwave index is significantly enhanced from 6.9 in SW0 up to 11 in SW3. The frequency response has also been simulated and is shown in Fig. 7(d). A constant microwave index and therefore wideband operation is achieved due to the low dispersion of the quasi-TEM propagation mode in the slow-wave CPW.

Characterization and Conclusions

In order to demonstrate the simulated performance, some of the previously designed slow-wave CPWs have been fabricated and characterized. The devices were fabricated on a silicon substrate covered with a 300 nm thick SiO₂ layer deposited using a plasma enhanced chemical vapor deposition (PECVD) process. The CPWs were formed with a lift-off process using TI35E photoresist in an image reversal process. The electrodes consist of 40 nm Ti, deposited through sputtering and 1000 nm Au, deposited through thermal evaporation. Figure 8 shows the obtained measurements results and the comparison with simulations. A multiline method has been applied to extract the microwave index from the slow-wave part of the CPW. The method uses a reference CPW (inset of Fig. 8(a)) in addition to the slow-wave CPW. A more detailed description can be found elsewhere^{30,31}.

Figure 8(a,b) show the variation of the microwave index and impedance in SW0 for values of w_2 varying from 10 μm to 100 μm , and the regular CPW (Fig. 3(a)), represented at $w_2=0 \mu\text{m}$. It can be seen that there is a good agreement with simulations. Figure 8(c) shows the measured microwave index for the regular CPW, SW0, SW2 and SW3. Also these results are in very good agreement with the simulations. The microwave index is improved from 2.36, 3.7 and 6.9 for the regular CPW, SW0 and SW2, respectively, up to 11.6 for SW3. An inset of Fig. 8(c) shows an optical image of the fabricated SW3. Additionally, Fig. 8(d) depicts the frequency response measured for a range up to 40 GHz.

Table 1 compares the obtained results in terms of microwave index, propagation losses and impedance with the values reported in the last two decades for slow-wave CPWs. The microwave index is largely increased for SW3 with respect to previous works. Furthermore, though propagation losses increase for SW3 with respect to SW0 and the regular CPW, the value remains comparable and even lower than the ones achieved in CPWs with an impedance of around 50 Ω .

In summary, we have demonstrated a design approach to increase the microwave index in CPWs. The proposed approach is based on the design of periodically distributed inductive and capacitive elements. A microwave index of 4.7 has been achieved by increasing the inductive behavior of the CPW with small slots on the ground and signal planes. In addition, the effect on the impedance has also been considered and it has been shown that it is possible to achieve high microwave indices while keeping the impedance around 50 Ω . Therefore, through the combination of inductive and capacitive elements, a microwave index up to 11.6 has been demonstrated. To the best of our knowledge, such value is the largest to date obtained in planar transmission lines.

Data availability. Requests for materials should be addressed to A.R.

References

- Wolff, I. Coplanar Microwave Integrated Circuits. <https://doi.org/10.1002/0470040882> (Wiley-Interscience, 2006).
- Pozar, D. M. Microwave engineering. *Addison-Wesley Publ. Co.* (1993).
- Selga, J., Velez, P., Bonache, J. & Martin, F. High miniaturization potential of slow-wave transmission lines based on simultaneous inductor and capacitor loading. 2017 47th European Microwave Conference (EuMC), Nuremberg, Germany. <https://doi.org/10.23919/EuMC.2017.8230964> (2017, October)

4. Wu, F. & Sun, L. Miniaturization of 4×4 Butler matrix using high slow-wave factor structure. 2017 IEEE 2nd Advanced Information Technology, Electronic and Automation Control Conference (IAEAC), Chongqing, China. <https://doi.org/10.1109/IAEAC.2017.8054317> (2017, March)
5. Naylor, J., Weller, T., Smith, M. & Culver, J. Slow-wave CPW slot-line transition. *IEE Proc. - Microwaves, Antennas Propag.* **152**, 297, <https://doi.org/10.1049/ip-map:20045109> (2005).
6. Hui, W. & Li, S. New Design of Delay Line Based on Slow-Wave Structure. 2017 4th International Conference on Information Science and Control Engineering (ICISCE), Changsha, China. <https://doi.org/10.1109/ICISCE.2017.324> (2017, July).
7. Yang, B., Qian, H. J., Shu, Y. & Luo, X. Compact bandpass filter with wide stopband using slow-wave CPW resonator with back-to-back coupled-scheme. 2017 IEEE International Symposium on Radio-Frequency Integration Technology, Seoul, South Korea. <https://doi.org/10.1109/RFIT.2017.8048274> (2017, August).
8. Kuo, C.-Y., Chen, A. Y.-K., Lee, C.-M. & Luo, C.-H. Miniature 60 GHz slow-wave CPW branch-line coupler using 90 nm digital CMOS process. *Electron. Lett.* **47**, 924 (2011).
9. Franc, A. L., Pistono, E., Meunier, G., Gloria, D. & Ferrari, P. A lossy circuit model based on physical interpretation for integrated shielded slow-wave CMOS coplanar waveguide structures. *IEEE Trans. Microw. Theory Tech.* **61**, 754–763, <https://doi.org/10.1109/TMTT.2012.2231430> (2013).
10. Miao, M. *et al.* Micromachined cavity-based bandpass filter and suspended planar slow-wave structure for vacuum-microelectronic millimeter-wave/THz microsystem embedded in LTCC packaging substrates. 2015 IEEE 65th Electronic Components and Technology Conference (ECTC), San Diego, USA. <https://doi.org/10.1109/ECTC.2015.7159837> (2015, May).
11. Sor, J., Qian, Y. & Itoh, T. Miniature low-loss CPW periodic structures for filter applications. in. *IEEE Transactions on Microwave Theory and Techniques* **49**, 2336–2341 (2001).
12. Ye, L. *et al.* Strongly Confined Spoof Surface Plasmon Polaritons Waveguiding Enabled by Planar Staggered Plasmonic Waveguides. *Sci. Rep.* **6**, 38528, <https://doi.org/10.1038/srep38528> (2016).
13. Tang, X. L. *et al.* Continuous Beam Steering Through Broadside Using Asymmetrically Modulated Goubau Line Leaky-Wave Antennas. *Sci. Rep.* **7**, <https://doi.org/10.1038/s41598-017-12118-8> (2017).
14. Kianinejad, A., Chen, Z. N. & Qiu, C. W. Design and modeling of spoof surface plasmon modes-based microwave slow-wave transmission line. *IEEE Trans. Microw. Theory Tech.* **63**, 1817–1825, <https://doi.org/10.1109/TMTT.2015.2422694> (2015).
15. Eleftheriades, G. V., Siddiqui, O. & Iyer, A. K. Transmission line models for negative refractive index media and associated implementations without excess resonators. *IEEE Microw. Wirel. Components Lett.* **13**, 51–53, <https://doi.org/10.1109/LMWC.2003.808719> (2003).
16. Caloz, C. & Itoh, T. Electromagnetic Metamaterials: Transmission Line Theory and Microwave Applications: The Engineering Approach, <https://doi.org/10.1002/0471754323> (2005).
17. Grbic, A. & Eleftheriades, G. V. Overcoming the Diffraction Limit with a Planar Left-Handed Transmission-Line Lens. *Phys. Rev. Lett.* **92**, <https://doi.org/10.1103/PhysRevLett.92.117403> (2004).
18. Alferness, R. C. Waveguide Electrooptic Modulators. *IEEE Trans. Microw. Theory Tech.* **30**, 1121–1137, <https://doi.org/10.1109/TMTT.1982.1131213> (1982).
19. Spickermann, R. & Dagli, N. Experimental analysis of millimeter wave coplanar waveguide slowwave structures on GaAs. *IEEE Trans. Microw. Theory Tech.* **42**, 1918–1924, <https://doi.org/10.1109/22.320774> (1994).
20. Motta, D. A. *et al.* Design of a 40 GHz Bandwidth Slow-Wave Silicon Modulator. 2017 SBMO/IEEE MTT-S International Microwave and Optoelectronics Conference (IMOC), Aguas de Lindoia, Brasil. <https://doi.org/10.1109/IMOC.2017.8121107> (2017, August).
21. Spickermann, R., Peters, M. G. & Dagli, N. A polarization independent GaAs-AlGaAs electrooptic modulator. *IEEE J. Quantum Electron.* **32**, 764–769, <https://doi.org/10.1109/3.492998> (1996).
22. A. Brimont, *et al.* High speed silicon electro-optical modulators enhanced via slow light propagation. *Opt. Express*, vol. **19**, no. 21, pp. 20876–85, <https://doi.org/10.1364/OE.19.020876> (Oct. 2011).
23. Shin, J., Sakamoto, S. R. & Dagli, N. Conductor loss of capacitively loaded slow wave electrodes for high-speed photonic devices. *J. Light. Technol.* **29**, 48–52, <https://doi.org/10.1109/JLT.2010.2091624> (2011).
24. Jaeger, N. A. & Lee, Z. K. Velocity-matched slow-wave electrodes for integrated electro-optic modulators. 20th International Congress on High Speed Photography and Photonics, Victoria, Canada. <https://doi.org/10.1117/12.145727> (1992, January).
25. Sakamoto, S., Spickermann, R. & Dagli, N. Narrow gap coplanar slow wave electrode for travelling wave electro-optic modulators. *Electron. Lett.* **31**, 1183–1185, <https://doi.org/10.1049/el:19950779> (1995).
26. Franc, A. L. *et al.* Slow-wave high performance shielded CPW transmission lines: A lossy model. 2009 European Microwave Conference (EuMC), Rome, Italy. <https://doi.org/10.1109/EUMC.2009.5296318> (2009, September).
27. Bautista, A., Franc, A. L. & Ferrari, P. Accurate Parametric Electrical Model for Slow-Wave CPW and Application to Circuits Design. *IEEE Trans. Microw. Theory Tech.* **63**, 4225–4235 (2015).
28. Simons, R. N. *Coplanar Waveguide Circuits, Components, and Systems*. <https://doi.org/10.1002/0471224758> (John Wiley & Sons, Inc., 2001).
29. He, D.-W. *et al.* An analytical model for coplanar waveguide on silicon-on-insulator substrate with conformal mapping technique. *Chinese Phys. B* **20**, 10210, <https://doi.org/10.1088/1674-1056/20/1/010210> (2011).
30. Engen, G. F. & Hoer, C. A. Thru-Reflect-Line: An Improved Technique for Calibrating the Dual Six-Port Automatic Network Analyzer. *IEEE Transactions on Microwave Theory and Techniques* **27**, 987–993, <https://doi.org/10.1109/TMTT.1979.1129778> (1979).
31. Rosa, A. *et al.* Barium titanate (BaTiO₃) RF characterization for application in electro-optic modulators. *Opt. Mater. Express* **7**, 4328–4336, <https://doi.org/10.1364/OME.7.004328> (2017).

Acknowledgements

This work has been supported by the European Commission through H2020-ICT-2015, n° 688544, L3MATRIX. Funding from project TEC2016-76849-C2-2-R (MINECO/FEDER, UE) is also acknowledged. Álvaro Rosa acknowledges the Spanish Ministry of Economy and Competitiveness for funding his grant.

Author Contributions

A.R. conceived the new designs, made the simulation and characterized the samples. S.V. fabricated the samples under the supervision of D.V.T. A.B. helped with the measurements and the analysis of the obtained results. The work was supervised by P.S. The paper was written by A.R. and reviewed by P.S. and D.V.T.

Additional Information

Competing Interests: The authors declare no competing interests.

Publisher's note: Springer Nature remains neutral with regard to jurisdictional claims in published maps and institutional affiliations.



Open Access This article is licensed under a Creative Commons Attribution 4.0 International License, which permits use, sharing, adaptation, distribution and reproduction in any medium or format, as long as you give appropriate credit to the original author(s) and the source, provide a link to the Creative Commons license, and indicate if changes were made. The images or other third party material in this article are included in the article's Creative Commons license, unless indicated otherwise in a credit line to the material. If material is not included in the article's Creative Commons license and your intended use is not permitted by statutory regulation or exceeds the permitted use, you will need to obtain permission directly from the copyright holder. To view a copy of this license, visit <http://creativecommons.org/licenses/by/4.0/>.

© The Author(s) 2018